Available online at www.sciencedirect.com
ScienceDirect
Ceramics International 38 (2012) 423–432
CERAMICS INTERNATIONAL
www.elsevier.com/locate/ceramint

Microstructure and physicomechanical properties of pressureless sintered multiwalled carbon nanotube/alumina nanocomposites

Soumya Sarkar, Probal Kr. Das *

Non-oxide Ceramics and Composites Division, Central Glass and Ceramic Research Institute (A CSIR Laboratory), Kolkata 700032, India

Received 18 April 2011; received in revised form 12 July 2011; accepted 12 July 2011
Available online 23rd July 2011

Abstract

Multiwalled carbon nanotube (MWCNT)/alumina (Al_2O_3) nanocomposites containing CNT from 0.15 vol.% to 2.4 vol.% have been successfully fabricated by simple wet mixing of as-received commercial precursors followed by pressureless sintering. Extent of densification of nanocomposites sintered at low temperature (e.g. 1500 °C) was <90%, but increased up to ~99% when sintered at 1700 °C and offered superior performance compared to pure Al_2O_3. Nanocomposites containing 0.3 vol.% MWCNT and sintered at 1700 °C for 2 h in Argon led to ~23% and ~34% improvement in hardness and fracture toughness, respectively, than monolithic Al_2O_3. In addition, the highest improvement (~20%) in bending strength was obtained for 0.15 vol.% MWCNT/Al_2O_3 nanocomposite compared to pure Al_2O_3. *Weibull* analysis indicated reliability of nanocomposites increased up to 0.3 vol.% MWCNT, whereas, beyond that loading consistency was the same as obtained for pure Al_2O_3. Detailed microstructure and fractographic analysis were performed to assess structure-property relationship of present nanocomposites.

Keywords: A. Sintering; B. Electron microscopy; B. Nanocomposites; C. Mechanical properties

1. Introduction

Carbon nanotubes having outstanding physicomechanical properties are presently considered as next generation reinforcing phase in polymers, metals and ceramics [1–5]. However, fabrication of a useful CNT reinforced nanocomposite also requires homogeneous filler dispersion, proper adhesion between filler and matrix and optimum interface properties [6,7]. Although, reports are available on CNT/polymer and CNT/metal nanocomposites fulfilling above mentioned features [2,3], for making structural CNT/ceramic nanocomposites particularly using Al_2O_3 which is the most ancient, widely available and cost-effective structural ceramic, major limitations are chemical incompatibility between these phases due to dissimilar bonding character and high clustering tendency of fibriform CNTs due to strong Van der Waals attractive forces and hydrophobicity [7,8]. Instead of contributing in property improvement, such agglomerated CNTs severely act as strength limiting defects in nanocomposites [9,10]. In literature, although, a variety of techniques have been proposed to improve dispersibility of CNTs in Al_2O_3 to enhance interface properties [6–20], these routes involved additional stringent steps, thus, limit easy processing and wider use of such nanocomposites. In addition, spark plasma sintering (SPS) [7–13] and hot-pressing (HP) [14–19] are the two techniques that have been commonly employed to densify CNT/Al_2O_3 nanocomposites. However, due to high cost involvement, incapability of continuous production and limited product shapes and sizes, SPS and HP are practically inappropriate for fabricating nanocomposites of various geometries having satisfactory performance at affordable price [20,21]. More surprisingly, even after employing above techniques, fabrication of CNT/Al_2O_3 nanocomposites with optimum CNT dispersion and maximum interface performance is still not achieved and significant divergences in available mechanical property data of CNT/Al_2O_3 nanocomposites have been noticed [6–19]. Zhang et al. [20] have recently prepared MWCNT/Al_2O_3 nanocomposites by pressureless sintering considering its commercial viability towards manufacturing of complex geometries to near net-shape using typical ceramic powder processing techniques. However, the initial precursor

* Corresponding author. Tel.: +91 33 2473 3469/76/77/96; fax: +91 33 2473 0957.
E-mail address: probal@cgcri.res.in (P.Kr. Das).

0272-8842/$36.00
doi:10.1016/j.ceramint.2011.07.023

treatment procedure adopted by Zhang et al. [20] was stringent comprising of concentrated acid purification and surface oxidation of as-received MWCNTs for ~27 h and ball milling of Al_2O_3 powder for 24 h. Furthermore, the freeze drying method used to prevent MWCNT segregation [20] is not a readily available technique in industrial field.

In this study an attempt was made to explore opportunities of fabricating structural MWCNT/Al_2O_3 nanocomposites having superior performance than pure Al_2O_3 by a simple and cost-effective process using commercial raw materials. To evade chances of strength limiting nanoscale defect formation on CNT surface by concentrated acid treatment [11,13], both MWCNT and Al_2O_3 were used directly in their as received state without any pre-treatment. In addition, normal air drying of MWCNT/Al_2O_3 slurry was employed instead of freeze drying. Nanocomposites containing five different CNT volume fractions from 0.15 vol.% to 2.40 vol.% were fabricated by wet mixing of as-received precursors followed by pressureless sintering in Argon atmosphere at three temperatures viz. 1500 °C, 1600 °C and 1700 °C. Nanocomposites were characterized in terms of density, apparent porosity, *Vickers* hardness, fracture toughness and four point bending strength. Microstructure of sintered and polished specimens and fractographic analyses of flexure tested specimens through gain boundary engineering were done to predict structure-property relationship. Properties were compared with pure Al_2O_3 to assess changes in performance of present nanocomposites.

2. Experimental procedures

2.1. Raw materials and sample preparation

MWCNT (>95 wt.% pure, *Shenzhen Nano Port Co., China*) and Al_2O_3 powder (*A-16-SG*, 99.8 wt.% pure) of *Almatis, ACC Ltd., India* were used in this study. Diameter and length of CNTs were between 60–100 nm and 5–15 μm, respectively. As per supplier's specification, surface area and average particle size of *A-16-SG* powder were 8.90 m^2/g and 0.5 μm, respectively.

At first, requisite MWCNT was dispersed in isopropyl alcohol using ultrasonic agitation for 1 h in an ultrasonic bath (*Oscar Ultrasonic Pvt. Ltd., India*). The dispersed slurry was then mixed with aqueous suspension of Al_2O_3 by magnetic stirring for 1–2 h followed by drying at 100 °C to remove volatiles and sieving through 60 mesh (B.S.) screen. Green billets were prepared by cold isostatic pressing at 150 MPa. Samples were finally sintered at 1500 °C, 1600 °C and 1700 °C for 2 h each in a graphite resistance heating furnace (*1000-4560-FP20*; *Thermal Tech. Inc., USA*) in static Argon (35–70 kPa) at a rate of 10 °C/min. Details of all batches evaluated in present work are given in Table 1.

Table 1
Details of MWCNT/Al_2O_3 batches.

Volume % MWNT added	Nomenclature	Theoretical density (g/cm^3)
0.00	*A0*	3.970
0.15	*A1*	3.967
0.30	*A2*	3.963
0.60	*A3*	3.957
1.20	*A4*	3.944
2.40	*A5*	3.917

2.2. Physical characterizations

Theoretical density of nanocomposites was calculated using *Rule of mixture* (Table 1). For that, density of MWCNTs (1.775 g/cm^3) was measured by pyknometer (*IS 1528:Part 9:1995*) and that of Al_2O_3 was taken as 3.97 g/cm^3 [11]. Density and apparent porosity of sintered samples were evaluated by *Archimedes* water immersion technique.

2.3. Mechanical characterizations

2.3.1. Bending strength

Room temperature bending strength was carried out as per ASTM *1161-02C* in a four point bending tester (*422, Netzsch-Geratebau GmbH, Germany*) at constant stress rate of 0.03 N/mm^2-s. Inner and outer span of test fixture was 20 mm and 40 mm, respectively. Bending modulus values were evaluated using standard formula [22]. 10 samples from each batch were tested to check repeatability of data.

2.3.2. Vickers hardness

Vickers hardness of sintered samples was evaluated using a micro-*Vickers* hardness tester (*402 MVD, Wolpert-Wilson, Germany*) at 9.8 N with 10 s dwell. 10 indents were made on each sample to verify consistency of data.

2.3.3. Fracture toughness

Indentation fracture toughness ($K_{IC,IF}$) of all samples was measured using direct crack measurement (*DCM*) method using formulations proposed by Niihara et al. [23–25] and Liang et al. [26]. Fracture toughness of specimens was also determined by single edge notched beam (*SENB*) method using ASTM *C-1421-09*. All tests were carried out in four-point bending instrument at constant stress rate of 0.03 N/mm^2-s. Ratio of notch depth (a) to specimen thickness (w) i.e. $\alpha = a/w$ was ranged from 0.35 to 0.60. Average fracture toughness ($K_{IC,SENB}$) was evaluated from 5 valid tests in which specimens were failed exactly from notched region.

2.4. Microstructure and fractographic analysis

Morphology of as-received MWCNTs has already been reported in our earlier work [27]. Effect of high temperature (1500 °C and 1700 °C in Argon) on structural stability of MWCNTs was studied using transmission electron microscope (TEM: *Tecnai G230 ST, FEI Company, The Netherlands*). Field emission scanning electron microscope (FESEM: *Supra-35, VP-Carl Zeiss, Germany*) was used to observe powder mixture homogeneity, microstructure of sintered and thermally etched specimens and fractographic analyses.

3. Results and discussion

3.1. Morphology of heat-treated MWCNTs

Figs. 1 and 2a indicate that after heat treatments at 1500 °C and 1700 °C in inert, the tubular texture of MWCNTs was favorably preserved with formation of internal bamboo structure that possibly formed during catalyst particle removal present in as-received MWCNTs [27]. High resolution TEM image of 1700 °C treated MWCNTs showed mostly parallel graphene layers and internal isolated compartments formed by bent graphene layers (Fig. 2b). Such bamboo-structured MWCNTs formed during high temperature exposure believed to offer better mechanical properties than hollow MWCNTs due to better connectivity with matrix, higher pull-out resistance and lower inner-wall slippage of the former in nanocomposites [28].

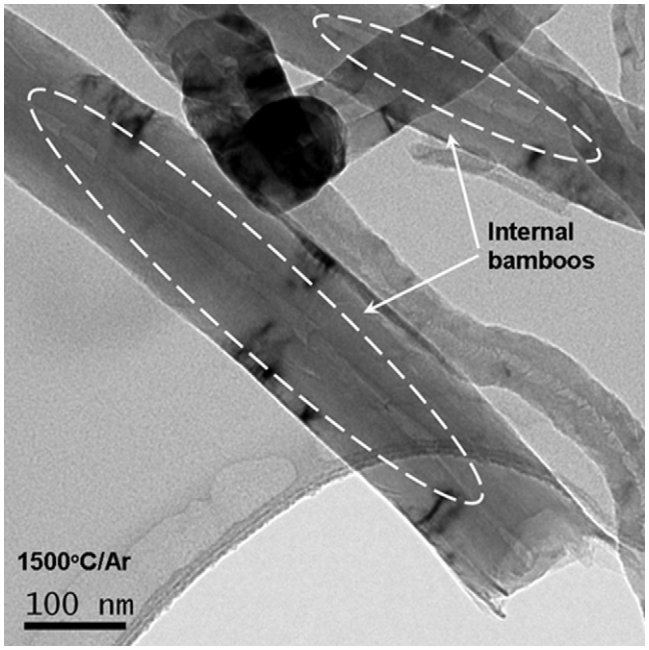

Fig. 1. TEM image of 1500 °C treated MWCNTs showing tubular structure and internal bamboos.

3.2. Microstructure and densification characteristics

As mentioned in earlier sections that in present study MWCNT was used directly in as received state and hence, they might had higher agglomeration i.e. clustering tendency in Al_2O_3 matrix as suggested by others [7,8,20]. Therefore, to minimize the effect of severe agglomeration of MWCNTs, we reinforced Al_2O_3 by MWCNTs from a low level i.e. from 0.15 vol.%. During FESEM studies of nanocomposite powder mixtures it was found that although in the lowest MWCNT containing batch most of the nanotubes were individually dispersed in Al_2O_3 matrix (Fig. 3a), with increasing CNT content, clustering of MWCNTs in matrix increased gradually due to enhanced effect of Van dar Waal's attraction force among tubes and eventually, majority of CNTs remained agglomerated in *A*5 (Fig. 3b).

Relative densities of sintered samples vs. sintering temperature are shown in Fig. 4. From the figure it is clear that while sintering at 1500 °C produced partially densified specimens, sintering at 1600 °C offered significant improvement in densification and finally, at 1700 °C, relative densities of *A*1, *A*2 and *A*3 batches were close to that of *A*0 (≥99% dense). A common trend of decreasing sinterability with increasing CNT loading was observed at each sintering temperature not only due to incorporation of light weight CNTs in Al_2O_3 (Table 1) but also due to porous rope-like structure of CNTs and poor solubilization [9,11,16,18]. The dual effect of sintering temperature and CNT content on densification of MWCNT/Al_2O_3 nanocomposites can be more clearly understood if we compare differential change (δ) of relative density and apparent porosity (*%AP*) of samples. Fig. 5(a and b) indicates that up to 0.6 vol.% MWCNT, only

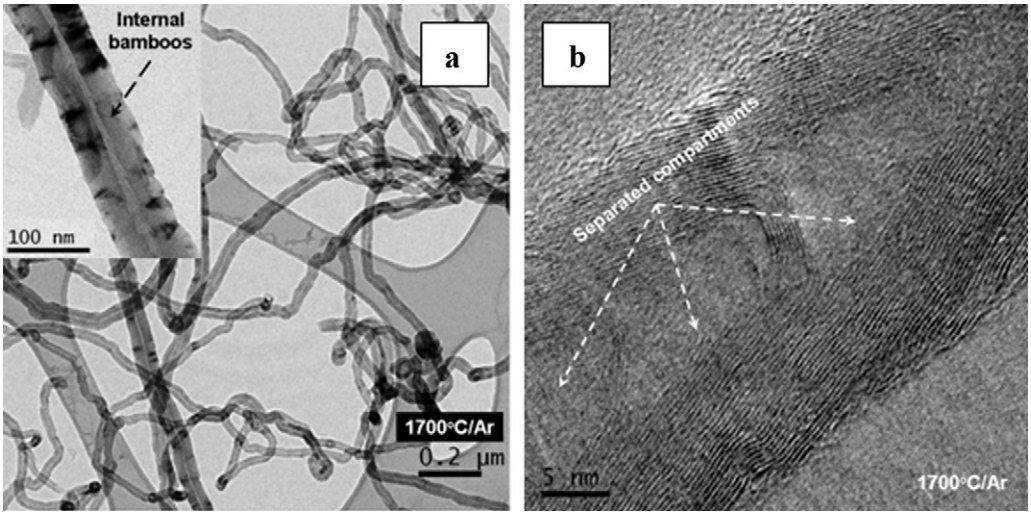

Fig. 2. (a) TEM image of 1700 °C treated MWCNTs having internal bamboo morphology (inset); (b) HRTEM image showing internal isolated compartments and mostly parallel external graphene layers.

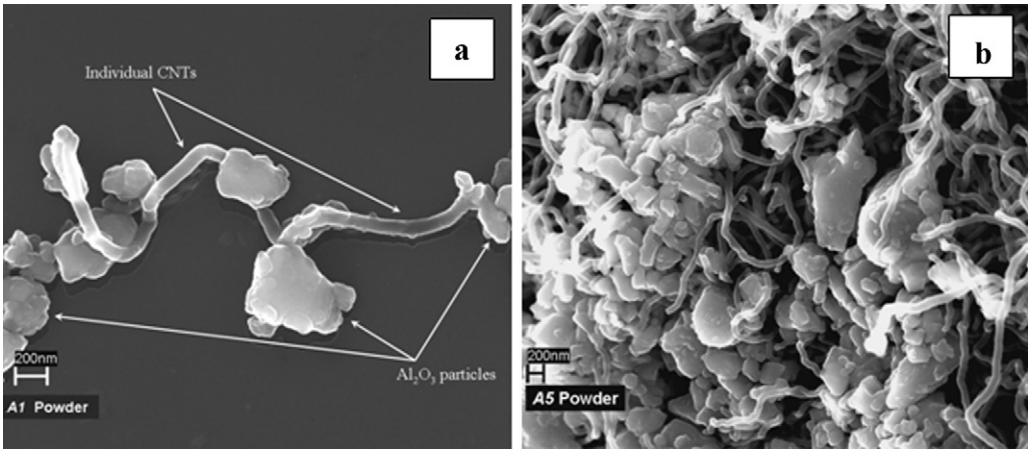

Fig. 3. Morphology of (a) *A*1 powder showing individual MWCNTs; (b) *A*5 powder showing agglomerated MWCNTs.

temperature played the primarily role in controlling sinterability of samples but beyond that, CNTs also had significant role in lowering consolidation of Al_2O_3 by restraining the process of pore removal and material transport through grain boundary even at high sintering temperatures. In addition, MWCNT aggregates, mainly in *A*4 and *A*5 batches, acted as pores of similar dimensions and played a negative role in densification and resulted in less dense, porous samples. Although, present results on densification data matched well with existing results on pure Al_2O_3 and MWCNT/Al_2O_3 nanocomposites prepared by various sintering techniques in 1500–1800 °C temperature range in different atmosphere [8–11,13–19,29–31], they differs from those reported by Zhang et al. [20] where pressureless sintering at 1500 °C for ≤2 h was sufficient to achieve relative density ∼100% for pure Al_2O_3 and ≥92% for MWCNT/Al_2O_3 nanocomposites up to 5 vol.% MWCNT possibly due to enhanced dispersion of filler as well as better filler/matrix interaction using modified precursors and much higher green density of specimens compacted at 310 MPa isostatic pressure. On contrary, pressureless sintering of pure Al_2O_3 with or without sintering additives and alumina matrix composites up to 1850 °C has been successfully employed by several researchers and reported enhancement in mechanical properties of such composites are good enough [29–41] to support the selected range of sintering temperature in present investigation. Further, considering TEM observations of heat-treated MWCNTs described in Section 3.1, it can be stated that MWCNT/Al_2O_3 nanocomposites can be successfully consolidated at high temperatures (at least up to 1700 °C) by pressureless sintering in inert without damaging structural stability of present MWCNTs. However, sintering of present CNT/Al_2O_3 nanocomposites beyond 1700 °C was not performed due to the following reason. It has been reported that Al_2O_3 in presence of carbon, undergoes carbothermal reduction and depending on reaction temperature and system pressure, reaction product may be either aluminum oxy-carbide (Al_2OC or Al_4O_4C) or aluminum carbide (Al_4C_3) [42]. Under reduced system pressure, low temperature (1500 °C ≤ T < 1700 °C) in Al_2O_3-C system is favorable for formation of Al_2OC due to size similarity between Al_2OC and Al_2O_3 molecules than Al_4O_4C. As interface, Al_2OC has chemical compatibility with both Al_2O_3 and CNT and forms a thin layer that is neither too strong nor too weak and favorable for making tougher MWCNT/Al_2O_3 nanocomposites [18]. On contrary, Al_4C_3 may destroy structural reliability of CNTs, therefore, is not desirable to fabricate tougher composites. As far as stability of MWCNTs is concerned, it has been reported that above 1700 °C, MWCNT may suffer from nanoscale corrugations by splitting and looping of external graphene layers [27] that can also adversely affect nanocomposite properties. Thus, keeping these in mind, sintering was restricted up to 1700 °C.

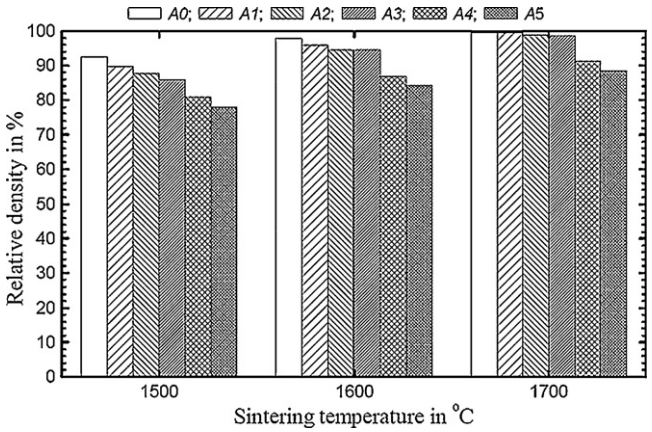

Fig. 4. Relative density of all samples after sintering at three sintering temperatures.

Microstructure of *A*0 sintered at 1500 °C for 2 h showed small under developed grains (1–2 μm) having pores of similar dimension (Fig. 6a). Sintering at 1600 °C resulted in dramatic decrease in porosity comprising well developed and nearly equiaxed Al_2O_3 grains of 4–5 μm (Fig. 6b). *A*0 sintered at 1700 °C showed further grain growth resulting in grain size between 4 μm and 12 μm (Fig. 6c). Microstructure of nanocomposites sintered at 1500 °C was similar to that of pure Al_2O_3. However, less porous regions were also observed (Fig. 6d). Nanocomposite containing 1.2 vol.% CNT sintered at 1600 °C showed dense microstructure having less void spaces (Fig. 6e). Presence of MWCNTs showed formation of smaller

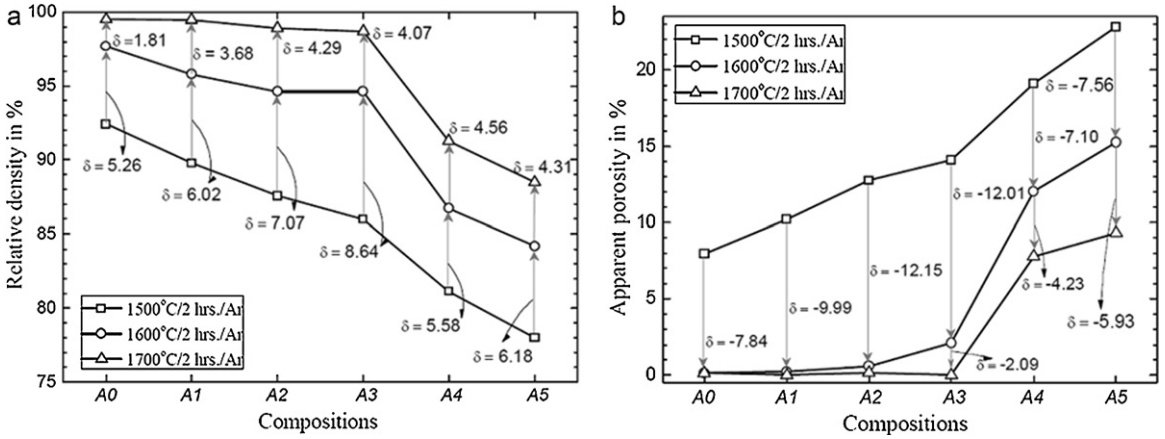

Fig. 5. Plot of (a) δ(RD) vs. compositions; (b) δ(%AP) vs. compositions sintered at different temperatures.

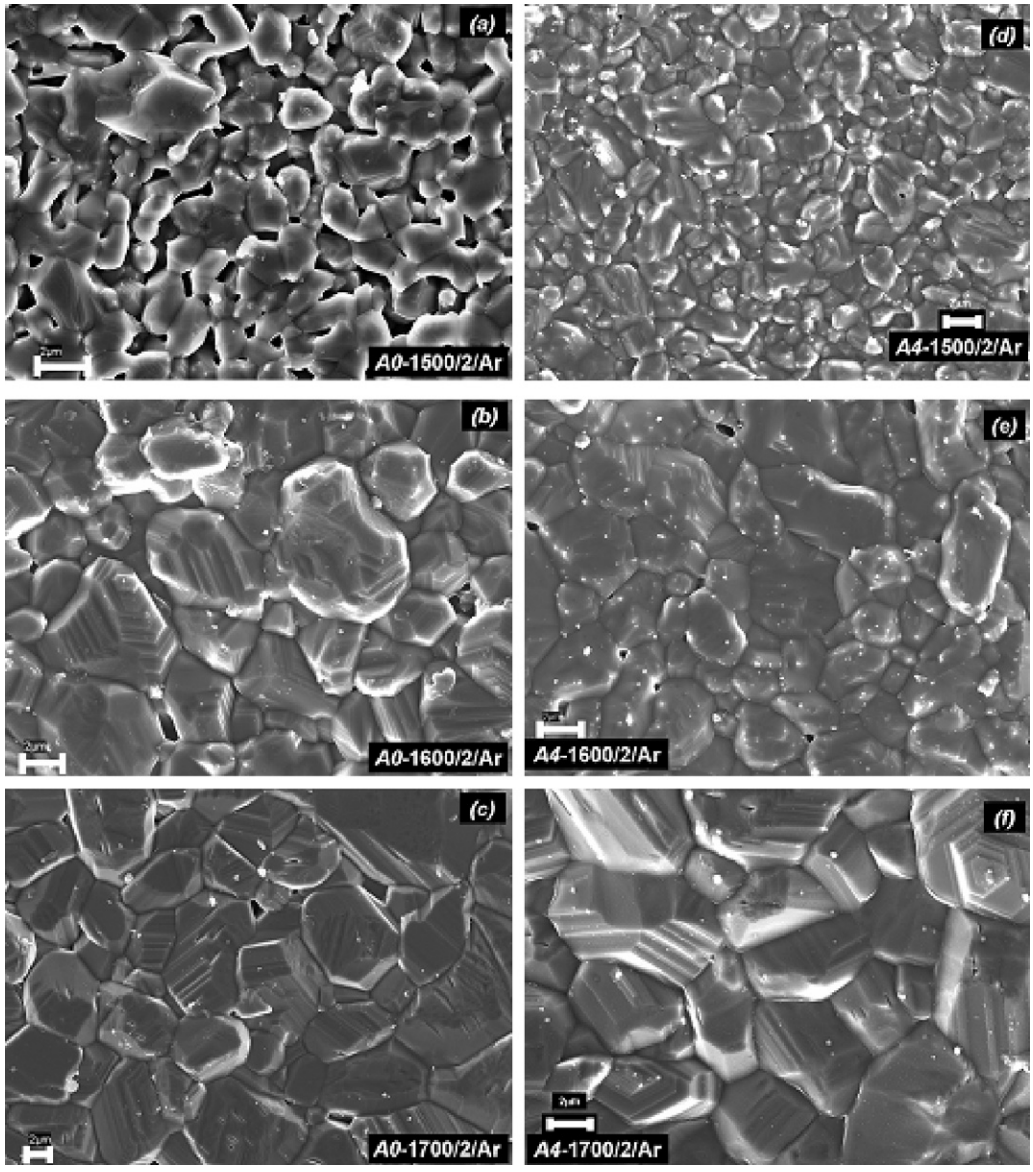

Fig. 6. Microstructures of (a–c) *A*0 and (d–f) *A*4 specimens sintered at different temperatures, scale: 2 μm.

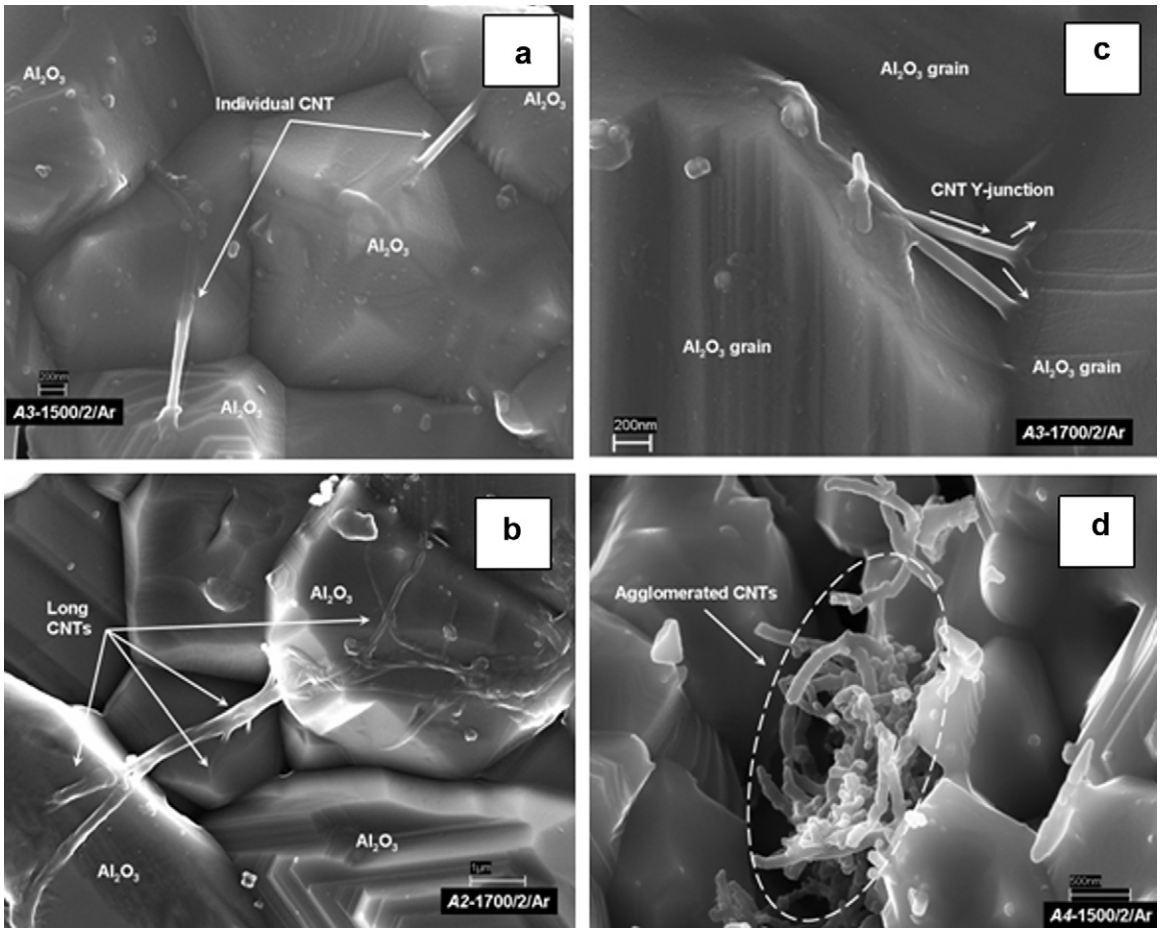

Fig. 7. Different MWCNT/Al_2O_3 interactions: (a) bridging of Al_2O_3 grains by individual CNTs; scale: 200 nm; (b) bundle of long MWCNTs; scale: 1 μm; (c) CNT Y-junctions; scale: 200 nm; (d) agglomerated CNTs at grain boundary; scale: 500 nm.

Al_2O_3 grains (1–3 μm) than pure Al_2O_3 sintered under identical condition (Fig. 6b). At 1700 °C, nanocomposites showed larger grains (2–8 μm) due to additional grain growth (Fig. 6f). Therefore, MWCNTs definitely possessed a grain refining effect for alumina matrix that could help in enhancing strength of resulting composites. During microstructure analysis of sintered nanocomposites, different CNT/Al_2O_3 interactions were also observed (Fig. 7(a–d)).

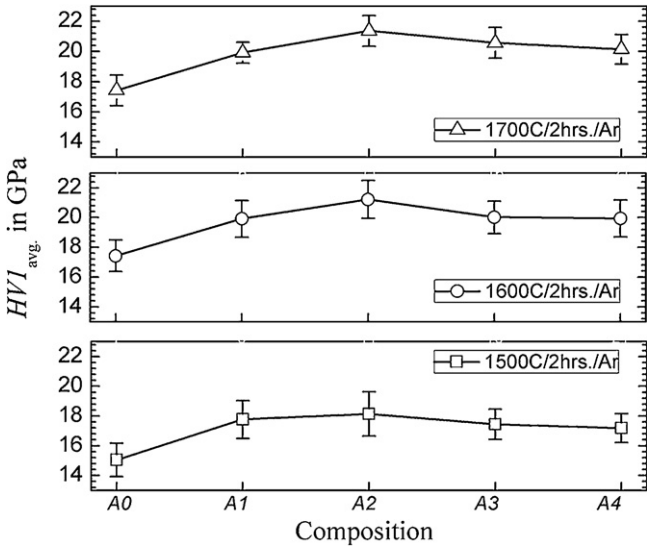

Fig. 8. *Vickers* hardness (*HV*1) of samples sintered at three temperatures.

3.3. Vickers hardness

Average *Vickers* hardness of all samples is plotted in Fig. 8. As discussed in Section 3.2 that sintering at 1500 °C produced porous samples having small under developed grains and thus, offered lower hardness and high scatter. Further, low sintering temperature also resulted in poor CNT/Al_2O_3 interface that led to insufficient load sharing between filler and matrix in nanocomposites. However, the excellent flexible nature coupled with very high energy absorption capability of MWCNTs offered 15–20% improvement in hardness even in these partially densified nanocomposites than pure Al_2O_3 (Fig. 8). Nanocomposites sintered at 1600 °C showed better hardness and lower scatter of experimental data due to sufficient densification and formation of better interface that ensure effective load sharing (Fig. 8). Hardness of nanocomposites sintered at 1600 °C increased up to 0.3 vol.% MWCNT and the highest value of ∼21 GPa was obtained for *A*2 which was ∼22% higher than *A*0. Nanocomposites with more than 0.3 vol.% CNT offered lower improvement

in hardness primarily due to the presence of clustered and non-uniformly dispersed CNTs that acted as defects with no load carrying ability and eventually, *A*4 specimen, offered ∼14% increase in *HV*1 than *A*0. Similarly, among 1700 °C sintered samples, the highest hardness (∼21 GPa) was obtained for *A*2. For *A*4 nanocomposite, hardness further increased with lower scatter of experimental data (Fig. 8) than that obtained after 1600 °C. *A*4 sample offered ∼16% higher hardness compared to *A*0 and this additional increase in hardness of *A*4 suggested that higher CNT loaded samples required higher sintering temperature to achieve better consolidation and proper interface performance. Interestingly, the extent of hardness improvement of present nanocomposites was higher than commonly found in literature [7,10–15,18,20] possibly because of homogeneous dispersion of MWCNTs at low loading especially up to 0.30 vol.%; large aspect ratio (i.e. length: diameter ratio) of present CNTs that successfully bridged several comparatively smaller sized Al_2O_3 grains (Fig. 7(a–c)) and helped in enhancing load bearing capacity of present nanocomposites. Due to lowest densification and presence of mostly agglomerated MWCNTs in *A*5 specimen, it was not possible to achieve required surface finish for *Vickers* hardness test and thus, only flexural strength measurement was performed.

3.4. Fracture toughness (K_{IC})

Indentation fracture toughness values of samples were measured from cracks produced by *Vickers* indentation. At an applied load of 9.8 N, most of the cracks had (*c*/*a*) ratio below 2.5 and thus, were *Palmqvist* in nature. However, in very few indents, cracks of median type having (*c*/*a*) ratio above 2.5 were also obtained. K_{IC} data of all samples evaluated using *DCM* and *SENB* methods are shown in Fig. 9(a–c) in which toughness data obtained by *Niihara* technique were moderately related with those obtained from *SENB* method. However, *Liang* method always produced sufficiently higher K_{IC} than *SENB* results. Such discrepancy in K_{IC} measured by *DCM* and *SENB* methods corroborates other reports [43,44]. As far as changes in K_{IC} of nanocomposites compared to pure Al_2O_3 was concerned, Fig. 9a shows, irrespective of toughness evaluation technique (*DCM* or *SENB*), except *A*4 specimen, all other nanocomposites had improved K_{IC} than pure Al_2O_3 densified at 1500 °C. However, scatter of individual K_{IC} data was high that indicated inconsistent toughening effect by CNTs in those partially densified nanocomposites. Sintering at 1600 °C offered additional enhancement in K_{IC} having better reproducibility indicating uniform toughening effect in nanocomposites

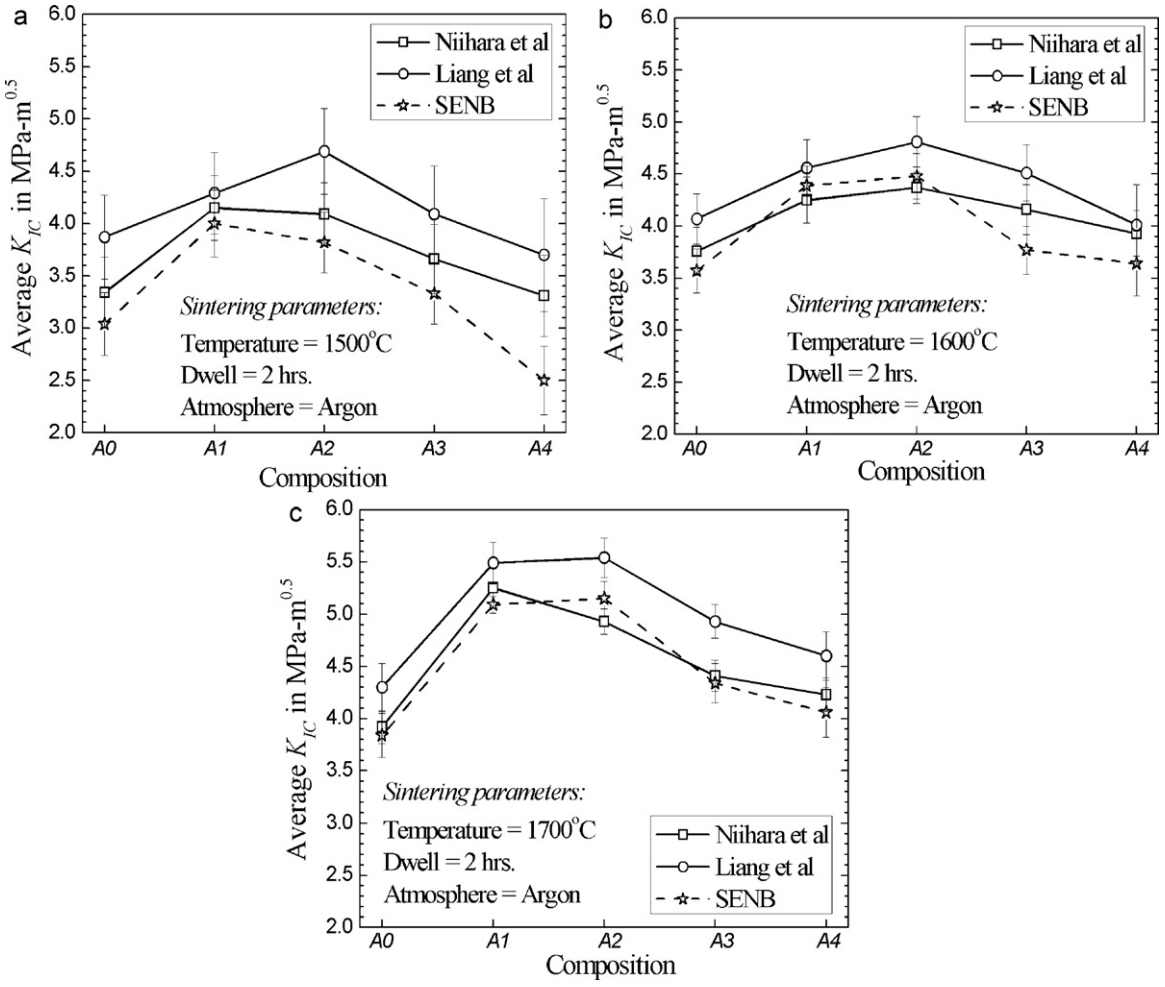

Fig. 9. Toughness (K_{IC}) of samples sintered at (a) 1500 °C; (b) 1600 °C; (c) 1700 °C.

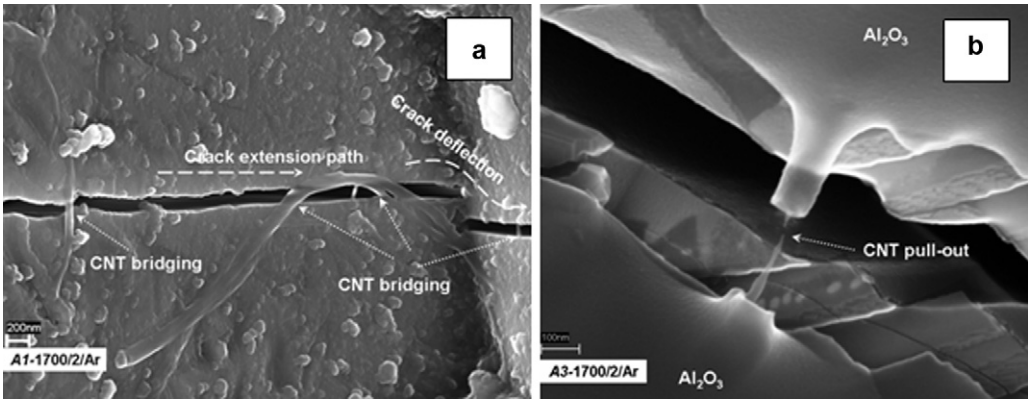

Fig. 10. (a) Crack bridging and deflection by MWCNTs; scale: 200 nm; (b) MWCNT pull-outs; scale: 100 nm.

(Fig. 9b). Similar observations were made in specimens sintered at 1700 °C (Fig. 9c). The highest K_{IC} evaluated from *DCM* and *SENB* technique was obtained for *A*2 specimen which was ∼34% higher than *A*0 sintered at 1700 °C. However, toughness of *A*4 specimen was still not improved much and was only 6–8% higher than that of pure Al_2O_3. Features like crack bridging and crack deflection by MWCNTs (Fig. 10a) and CNT pull-outs (Fig. 10b) were observed indicating presence of useful CNT/Al_2O_3 interface for load sharing and effective fracture energy dissipation. The extensive bamboo structure formed during high temperature exposure of MWCNTs (Section 3.1) also contributed in toughness improvement by providing structural anchors to improve matrix/filler connectivity and lowering the so called "*telescopic effect*" of MWCNTs thereby increasing the pull-out resistance compared to hollow MWCNTs having smooth external surface [28]. Although, improvement in K_{IC} (6–34%) of present nanocomposites matched favorably with available literature data [7,10–12,19,20], in some cases the increase was also found to be lower than achieved particularly in hot-pressed or spark plasma sintered nanocomposites [8,15–18]. However, the observed discrepancy in extent of toughness improvement in CNT/Al_2O_3 nanocomposites is quite common and reasons behind this are not straightforward because several issues contribute in this including purity and aspect ratio of CNT used, CNT orientation, surface characteristics of filler and matrix, sintering technique, interface composition and thickness, bridging characteristics, residual stress field around filler and matrix and also matrix grain size. Therefore, involvement of each of these features finally resulted in observed K_{IC} of nanocomposite.

3.5. Bending strength and modulus

From Fig. 11, it may be visualized that up to 0.6 vol.% MWCNT loading, nanocomposites had higher bending strength compared to *A*0 (∼225 MPa). Bending strength values of present specimens including pure Al_2O_3 were lower than normally found in recent literature [9,11,15,16,18–20] possibly due to densification of alumina without any sintering additive and low green body compaction that required higher sintering temperature for complete densification and resulted in larger grain size that ultimately reduced flexural strength of present specimens. However, this should not minimize the primary interest in assessing the extent of strength improvement of present nanocomposites compared to pure alumina. While, the highest strength was obtained for *A*1 (∼265 MPa), *A*2 and *A*3 offered ∼12% and ∼6% higher strength, respectively, than *A*0. However, strength of *A*4 and *A*5 nanocomposites were ∼45% and ∼70% lower, respectively, than pure Al_2O_3. Similarly, while, the highest modulus was obtained for *A*2 (∼20% higher than *A*0), *A*5 had ∼15% lower modulus than that obtained for pure Al_2O_3 (Fig. 11). However, from Fig. 11 it may also be visualized that in *A*4 and *A*5 specimens, both strength and modulus value had comparatively lower scatter of data than others possibly due to the fact that at high MWCNT content, presence of characteristically agglomerated CNTs and poor interface throughout the specimen resulted in failure having less variation within samples tested. *Weibull* modulus values (in parenthesis of Fig. 11) evaluated using 2-parameter *Weibull* statistics [45] indicated that while nanocomposites containing up to 0.3 vol.% MWCNT had less flaw sensitivity than monolithic Al_2O_3, consistency of strength data beyond that was the same as obtained for pure Al_2O_3. Fractographic studies revealed that fracture of pure Al_2O_3 and nanocomposites were primarily originated from surface flaws followed by crack propagation (Fig. 12(a and b)). Presence of bridging and

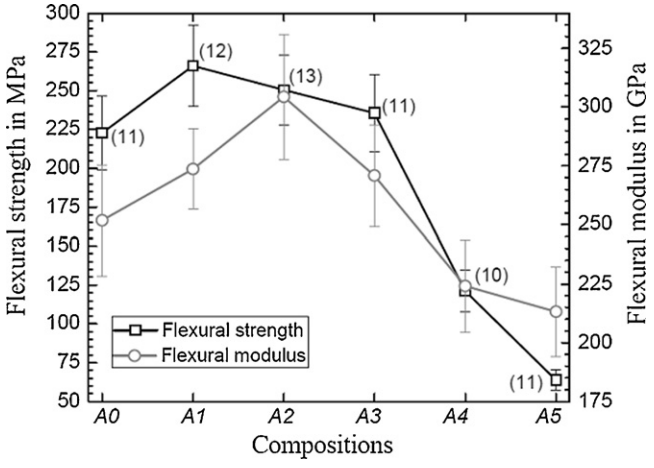

Fig. 11. Room temperature bending strength and modulus of samples.

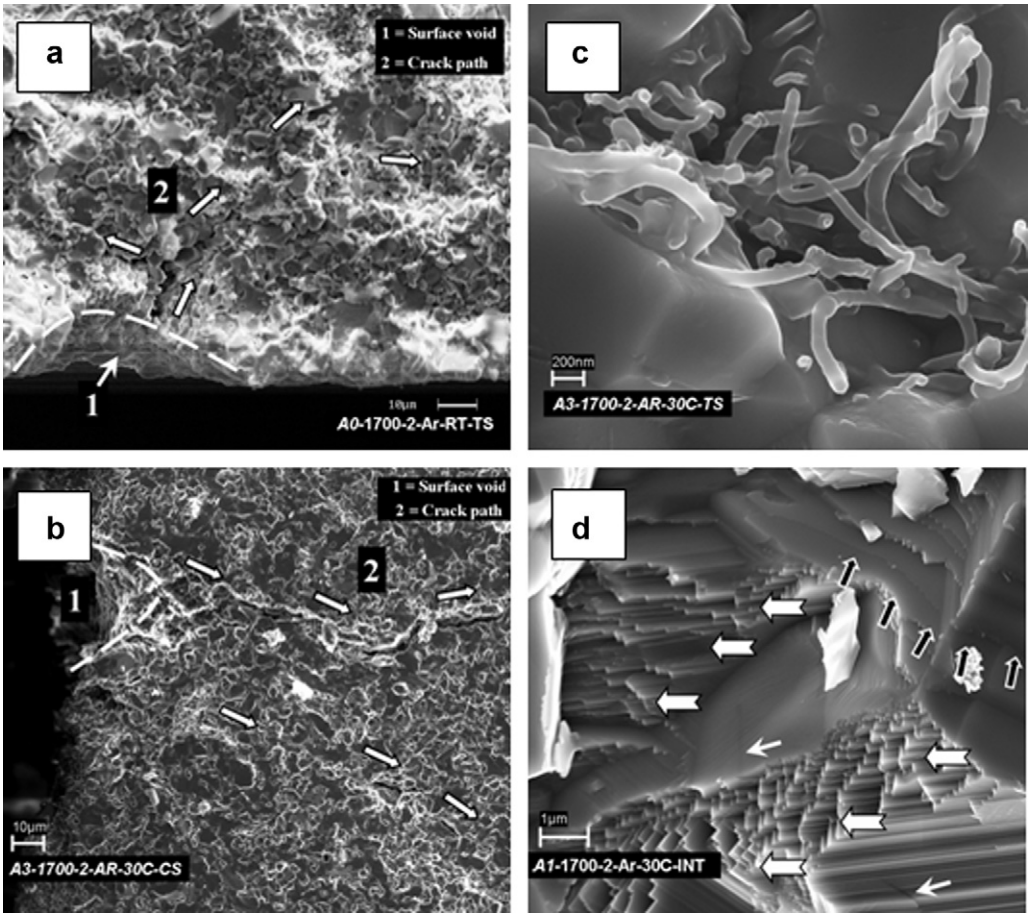

Fig. 12. Fractographs of flexure tested samples (a–b) primary failure site in pure Al_2O_3 and nanocomposites; (c) bridging and pulled-out CNTs along grain boundary of *A*3 specimen; (d) grain failure modes in *A*1 nanocomposite.

pulled-out nanotubes along grain boundary regions was also observed in nanocomposites (Fig. 12c). Detailed fractographic observation revealed that failure at individual matrix grains in nanocomposites involved features like shear induced slip band formation (white arrows in Fig. 12d), regions of localized deformation (black arrows in Fig. 12d) and intra-granular crack propagation (thin white arrows in Fig. 12d).

4. Conclusions

It is possible to fabricate MWCNT/Al_2O_3 nanocomposites by simple wet mixing of as-received commercial grade precursors without any purification and/or surface modification steps of the raw materials followed by pressureless sintering without damaging structural integrity of MWCNTs. Further, during sintering at high temperature (e.g. 1700 °C in inert) formation of extensive internal bamboo morphology in reinforcing MWCNTs contributed considerably in improving mechanical properties of present nanocomposites. Nanocomposites containing up to 0.6 vol.% MWCNT extend better reinforcing effects in structural Al_2O_3. Improved mechanical performance of nanocomposites was achieved by homogeneous dispersion of CNTs up to 0.6 vol.%, proper densification of matrix containing grains of lower size than sintered pure Al_2O_3 and better interface performance. The well-distributed MWCNTs aligned both parallel and perpendicular to crack plane helped in successful crack bridging, crack deflection and nanotube pull-out that resulted in improved mechanical properties of these low cost MWCNT/Al_2O_3 nanocomposite.

Acknowledgements

Authors express sincere gratitude to the Director, *Central Glass and Ceramic Research Institute (CG&CRI), India* for his kind permission to publish this work. Authors are also grateful to members of *Analytical Facility Division, CG&CRI*, for their extensive help during microstructure analysis. First author acknowledges the financial support of the Council of Scientific and Industrial Research (CSIR), India.

References

[1] R.H. Baughman, A.A. Zakhidov, W.A.D. Heer, Carbon nanotubes-the route toward applications, Science 297 (2002) 787–792.
[2] D. Luo, W.-X. Wang, Y. Takao, Effects of the distribution and geometry of carbon nanotubes on the macroscopic stiffness and microscopic stresses of nanocomposites, Compos. Sci. Technol. 67 (2007) 2947–2958.
[3] S.R. Bakshi, D. Lahiri, A. Agarwal, Carbon nanotube reinforced metal matrix composites – a review, Int. Mater. Rev. 55 (2010) 41–64.
[4] S.S. Samal, S. Bal, Carbon nanotube reinforced ceramic matrix composites – a review, J. Miner. Mater. Charact. Eng. 7 (2008) 355–370.

[5] R.S. Ruoff, D. Qian, W.K. Liu, Mechanical properties of carbon nanotubes: theoretical predictions and experimental measurements, C. R. Physique 4 (2003) 993–1008.
[6] Z. Xia, L. Riester, W.A. Curtin, H. Li, B.W. Sheldon, J. Liang, B. Chang, J.M. Xu, Direct observation of toughening mechanisms in carbon nanotube ceramic matrix composites, Acta Mater. 52 (2004) 931–944.
[7] J. Sun, L. Gao, W. Li, Colloidal processing of carbon nanotube/alumina composites, Chem. Mater. 14 (2002) 5169–5172.
[8] M. Estili, A. Kawasaki, H. Sakamoto, Y. Mekuchi, M. Kuno, T. Tsukada, The homogeneous dispersion of surfactantless, slightly disordered, crystalline, multiwalled carbon nanotubes in α-alumina ceramics for structural reinforcement, Acta Mater. 56 (2008) 4070–4079.
[9] G. Yamamoto, M. Omori, K. Yokomizo, T. Hashida, Mechanical properties and structural characterization of carbon nanotube/alumina composites prepared by precursor method, Diam. Rel. Mater. 17 (2008) 1554–1557.
[10] C.B. Mo, S.I. Cha, K.T. Kim, K.H. Lee, S.H. Hong, Fabrication of carbon nanotube reinforced alumina matrix nanocomposite by sol–gel process, Mater. Sci. Eng. A 395 (2005) 124–128.
[11] G. Yamamoto, M. Omori, T. Hashida, H. Kimura, A novel structure for carbon nanotube reinforced alumina composites with improved mechanical properties, Nanotechnology 19 (2008) 315708.
[12] T. Zhang, L. Kumari, G.H. Du, W.Z. Li, Q.W. Wang, K. Balani, A. Agarwal, Mechanical properties of carbon nanotube–alumina nanocomposites synthesized by chemical vapor deposition and spark plasma sintering, Compos. Part A 40 (2009) 86–93.
[13] A.C. Zaman, C.B. Üstündag, A. Celik, A. Kara, F. Kaya, C. Kaya, Carbon nanotube/boehmite-derived alumina ceramics obtained by hydrothermal synthesis and spark plasma sintering (SPS), J. Eur. Ceram. Soc. 30 (2010) 3351–3356.
[14] J.-W. An, D.-S. Lim, Effect of carbon nanotube additions on the microstructure of hot-pressed alumina, J. Ceram. Process. Res. 3 (2002) 201–204.
[15] I. Ahmad, H. Cao, H. Chen, H. Zhao, A. Kennedy, Y.Q. Zhu, Carbon nanotube toughened aluminium oxide nanocomposite, J. Eur. Ceram. Soc. 30 (2010) 865–873.
[16] J. Fan, D. Zhao, M. Wu, Z. Xu, J. Song, Preparation and microstructure of multi-wall carbon nanotubes-toughened Al_2O_3 composite, J. Am. Ceram. Soc. 89 (2006) 750–753.
[17] T. Wei, Z. Fan, G. Luo, F. Wei, A new structure for multi-walled carbon nanotubes reinforced alumina nanocomposite with high strength and toughness, Mater. Lett. 62 (2008) 641–644.
[18] I. Ahmad, M. Unwin, H. Cao, H. Chen, H. Zhao, A. Kennedy, Y.Q. Zhu, Multi-walled carbon nanotubes reinforced Al_2O_3 nanocomposites: mechanical properties and interfacial investigations, Compos. Sci. Technol. 70 (2010) 1196–1199.
[19] J. Sun, L. Gao, X. Jin, Reinforcement of alumina matrix with multi-walled carbon nanotubes, Ceram. Int. 31 (2005) 893–896.
[20] S.C. Zhang, W.G. Fahrenholtz, G.E. Hilmas, E.J. Yadlowsky, Pressureless sintering of carbon nanotube–Al_2O_3 composites, J. Eur. Ceram. Soc. 30 (2010) 1373–1380.
[21] A. Mukhopadhyay, B. Basu, Consolidation–microstructure–property relationships in bulk nanoceramics and ceramic nanocomposites: a review, Int. Mater. Rev. 52 (2007) 257–288.
[22] F. Mujika, On the difference between flexural moduli obtained by three-point and four-point bending tests, Polym. Test. 25 (2006) 214–220.
[23] K. Niihara, R. Morena, D.P.H. Hasselman, Evaluation of K_{IC} of brittle solid by the indentation method with low crack-to-indent ratios, J. Mater. Sci. Lett. 1 (1982) 13–16.
[24] K. Niihara, R. Morena, D.P.H. Hasselman, in: R.C. Bradt, A.G. Evans, D.P.H. Hasselman, F.F. Lange (Eds.), Fracture Mechanics of Ceramics, vol. 5, Plenum, New York, 1983, p. 97.
[25] K. Niihara, R. Morena, D.P.H. Hasselman, Further reply to comment on elastic/plastic indentation damage in ceramics: the median/radial crack system, J. Am. Ceram. Soc. 65 (1982) C116–C118.
[26] K.M. Liang, G. Orange, G. Fantozzi, Evaluation by indentation of fracture toughness of ceramic materials, J. Mater. Sci. 25 (1990) 207–214.
[27] S. Sarkar, P.K. Das, S. Bysakh, Effect of heat treatment on morphology and thermal decomposition kinetics of multiwalled carbon nanotubes, Mater. Chem. Phys. 125 (2011) 161–167.
[28] M. Olek, J. Ostrander, S. Jurga, H. Mohwald, N. Kotov, K. Kempa, M. Giersig, Layer-by-layer assembled composites from multiwall carbon nanotubes with different morphologies, Nano Lett. 4 (2004) 1889–1895.
[29] S. Junlong, L. Changxia, Z. Xihua, W. Baowei, N. Xiuying, Effect of diopside addition on sintering and mechanical properties of alumina, Ceram. Int. 35 (2009) 1321–1325.
[30] K. Maiti, A. Sil, Relationship between fracture toughness characteristics and morphology of sintered Al_2O_3 ceramics, Ceram. Int. 36 (2010) 2337–2344.
[31] K. Vishista, F.D. Gnanam, Effect of strontia on the densification and mechanical properties of sol–gel alumina, Ceram. Int. 32 (2006) 917–922.
[32] O. Abe, S. Takata, Y. Ohwa, Toughening of NiAl–alumina composites by self-constructed compressive surface layers under oxidation, J. Eur. Ceram. Soc. 24 (2004) 489–494.
[33] K.F. Cai, D.S. McLachlan, N. Axen, R. Manyatsa, Preparation, microstructures and properties of Al_2O_3–TiC composites, Ceram. Int. 28 (2002) 217–222.
[34] G.A. Carter, A.V. Riessen, R.D. Hart, Wear of zirconia-dispersed alumina at ambient temperature, 140 °C and 250 °C, J. Eur. Ceram. Soc. 26 (2006) 3547–3555.
[35] D. Galusek, J. Sedlacek, R. Riedel, Al_2O_3–SiC composites prepared by warm pressing and sintering of an organosilicon polymer-coated alumina powder, J. Eur. Ceram. Soc. 27 (2007) 2385–2392.
[36] H. Miyazaki, Y.-I. Yoshizawa, K. Hirao, Preparation and mechanical properties of 10 vol.% zirconia/alumina composite with fine-scale fibrous microstructure by co-extrusion process, Mater. Lett. 58 (2004) 1410–1414.
[37] P.G. Rao, M. Iwasa, T. Tanaka, I. Kondoh, T. Inoue, Preparation and mechanical properties of Al_2O_3–15 wt.%ZrO_2 composites, Scripta Mater. 48 (2003) 437–441.
[38] H. Reveron, O. Zaafrani, G. Fantozzi, Microstructure development, hardness, toughness and creep behaviour of pressureless sintered alumina/SiC micro–nanocomposites obtained by slip-casting, J. Eur. Ceram. Soc. 30 (2010) 1351–1357.
[39] R. Torrecillas, M. Schehl, L.A. Diaz, Creep behaviour of alumina–mullite–zirconia nanocomposites obtained by a colloidal processing route, J. Eur. Ceram. Soc. 27 (2007) 4613–4621.
[40] W.H. Tuan, R.Z. Chen, T.C. Wang, C.H. Cheng, P.S. Kuo, Mechanical properties of Al_2O_3/ZrO_2 composites, J. Eur. Ceram. Soc. 22 (2002) 2827–2833.
[41] H. Sarraf, R. Herbig, M. Maryska, Fine-grained Al_2O_3–ZrO_2 composites by optimization of the processing parameters, Scripta Mater. 59 (2008) 155–158.
[42] J.H. Cox, L. Pidgeon, An investigation of the aluminum–oxygen–carbon system, Can. J. Chem. 41 (1963) 671–683.
[43] E. Rudnayová, J. Dusza, M. Kupková, Comparison of fracture toughness measuring methods applied on silicon nitride ceramics, J. Phys. IV 3 (1993) 1273–1276.
[44] H. Miyazaki, H. Hyuga, K. Hirao, T. Ohji, Comparison of fracture resistance as measured by the indentation fracture method and fracture toughness determined by the single-edge-precracked beam technique using silicon nitrides with different microstructures, J. Eur. Ceram. Soc. 27 (2007) 2347–2354.
[45] S. Sarkar, A. Dey, P.K. Das, A.K. Mukhopadhyay, A. Kumar, Evaluation of micromechanical properties of carbon/carbon and carbon/carbon–silicon carbide composites at ultralow load, Int. J. Appl. Ceram. Technol. 8 (2011) 282–297.